14. C. Dry, *Comp. Struct.* **35**, 263 (1996).
15. L. P. Engle, K. B. Wagener, *J. Macromol. Sci. Rev. Macromol. Chem.* **C33 (3)**, 239 (1993).
16. J. P. Kennedy, K. F. Castner, *J. Polym. Sci., Polym. Chem. Ed.* **17**, 2039 (1979).
17. Y. Chujo, K. Sada, T. Saegusa, *Macromolecules* **23**, 2636 (1990).
18. J. R. Jones, C. L. Liotta, D. M. Collard, D. A. Schiraldi, *Macromolecules* **32**, 5786 (1999).
19. Y. Imai, H. Itoh, K. Naka, Y. Chujo, *Macromolecules* **33**, 4343 (2000).
20. J. R. McElhanon, D. R. Wheeler, *Org. Lett.* **3**, 2681 (2001)
21. C. Goussé, A. Gandini, P. Hodge, *Macromolecules* **31**, 314 (1998).
22. The synthesis procedures for compounds **1** (liquid at 24°C) and **2** (mp, 113° to 114°C) and for polymer **3** are available in the supplemental material, available on *Science* Online at www.sciencemag.org/cgi/content/full/295/5560/1698/DC1.
23. B. Rickborn, *Org. React.* **52**, 1 (1998).
24. J. M. Barton, *Adv. Polym. Sci.* **72**, 111 (1985).
25. N. S. Isaacs, *Physical Organic Chemistry* (Longman Scientific and Technical, 1997).
26. R. C. McMaster, Ed., *Nondestructive Testing Handbook* (American Society for Nondestructive Testing, ed. 2, 1982). The ultrasonics method takes advantage of the direct relation between mechanical properties (Young's modulus) and the propagation velocity of ultrasound through the material.
27. Whereas in the solid state the reversibility is observable only to the extent of ~ 10% to 20% (see Fig. 4, A and B), a suspension of a 350 mg sample of a monolith in 50 ml chlorobenzene dissolved completely upon heating to reflux over ~1 hour.
28. M. Ribeiro, J.-P. E. Grolier, *J. Therm. Anal. Cal.* **57**, 253 (1999).
29. M. Pyda, B. Wunderlich, *J. Polym. Sci. Polym. Phys. Ed. B* **38**, 622 (2000).
30. M. Song, *J. Therm. Anal. Cal.* **63**, 699 (2001).
31. The compact tension test specimens were made according to the literature [Y. Murakami, Ed., *Stress Intensity Factors Handbook* (Pergamon, Tokyo, 1987), vol. 1, p. 18], with $W = 12$ mm, $t = 6$ mm and $a/W \approx 0.4$, where W is width, t is thickness, and a is length of notch. The fracture toughness (K_{Ic}) can be determined as $K_{Ic} = \alpha P_c$ where α is a geometry and materials property, which can be calculated from the equation shown in the work cited in this reference, and P_c is the critical load at fracture (*4*). α was measured to be 1.1×10^4 $m^{-3/2}$. The fracture energy (G_{Ic}) value can be calculated according to the literature (*7*), $G_{Ic} = (1 - \nu^2) K_{Ic}^2/E$, where ν is the Poisson ratio and E is Young's modulus. Therefore, in terms of fracture energy, the best value of re-mending efficiency was 32%, and the average efficiency for a number of specimens (after thermal treatment at 150°C) was 25%.
32. J. E. Mark, Ed., *Polymer Data Handbook* (Oxford Univ. Press, New York, 1999), pp. 91 and 464.
33. We thank NSF for support through a grant (DMR 976302). We also thank J. R. Heath and R. Beckman for SEM images, W. P. Weber for thermal mechanical analysis, and C. E. Hoyle and C. Nguyen for constructive discussions on the synthesis of compounds with maleimide moieties.

30 August 2001; accepted 30 January 2002

Protein Nanoarrays Generated By Dip-Pen Nanolithography

Ki-Bum Lee,[1] So-Jung Park,[1] Chad A. Mirkin,[1]* Jennifer C. Smith,[2] Milan Mrksich[2]*

Dip-pen nanolithography was used to construct arrays of proteins with 100- to 350-nanometer features. These nanoarrays exhibit almost no detectable nonspecific binding of proteins to their passivated portions even in complex mixtures of proteins, and therefore provide the opportunity to study a variety of surface-mediated biological recognition processes. For example, reactions involving the protein features and antigens in complex solutions can be screened easily by atomic force microscopy. As further proof-of-concept, these arrays were used to study cellular adhesion at the submicrometer scale.

Arrays of microscopic features comprising different proteins are extremely important for proteomics and cell research, pharmaceutical screening processes (*1–4*), and panel immunoassays (*5, 6*). Many conventional patterning techniques, including photolithography (*6, 7*), microcontact printing (*2, 8*), and spot arraying (*1*), have been used for fabricating such arrays. Submicrometer spot arrays of proteins have been generated by finely focused ion beam lithography (FFIB) (*9*), and individual micrometer and submicrometer features have been prepared by atomic force microscopy (AFM) techniques with varying degrees of success (*10–14*). One of the advantages of miniaturization is that when a feature composed of receptors is miniaturized to the scale of the biological analytes, new methods for screening reactions involving such receptors and analytes become available, because almost every physical property of the receptor feature is changed upon reaction with the analyte, including the height, hydrophobicity, roughness, and shape of each feature, which are all variables easily probed with a conventional AFM. One disadvantage of receptor feature miniaturization in such an array is that nonspecific binding of the protein array can become a major problem leading to large background signals. For example, it could be difficult to differentiate inactive areas of the substrate that experience such binding from the active receptor features, thereby complicating the analysis of the nanoscale libraries. Indeed, others who have attempted to study reactions involving antibodies and antigens on a surface with an AFM have noted the importance of eliminating nonspecific binding when studying individual nano- and micrometer-scale protein features (*10–13*). Here, we describe how a high-resolution patterning technique, dip-pen nanolithography (DPN), can be used to construct nanoarrays of proteins. Moreover, we demonstrate that these arrays can be fabricated with almost no detectable nonspecific binding of proteins to the passivated portions of the array, even in solutions containing multiple proteins, and that reactions involving the protein features and antigens can be screened by AFM. Finally, we show how such nanoarrays can be implemented in the study of cellular interactions with nanopatterned surfaces.

A typical protein array was fabricated by initially patterning 16-mercaptohexadecanoic acid (MHA) on a gold thin-film substrate in the form of dots or grids. The features studied thus far, both lines and dots, have been as large as 350 nm (line width and dot diameter, respectively) and as small as 100 nm (Fig. 1). The areas surrounding these features were passivated with 11-mercaptoundecyl-tri(ethylene glycol) by placing a droplet of a 10 mM ethanolic solution of the surfactant on the patterned area for 45 min followed by copious rinsing with ethanol and, then, NANOpure water (NANOpure, Barnstead/Thermolyne Corp.). As proof-of-concept experiments, the proteins were absorbed on the preformed MHA patterns (Fig. 2) by immersing the substrate in a solution containing the desired protein (10 μg/ml) for 1 hour. The substrate was then removed and rinsed with 10 mM Tris buffer [Tris-(hydroxymethly) aminomethane], Tween-20 solution (0.05%) and, finally, NANOpure water. Such proteins have a high affinity for carboxylic acid–terminated monolayers at pH 7 (*10–13*) and a relatively weak affinity for surfaces coated with 11-mercaptoundecyl-tri(ethylene glycol) (*15, 16*). The protein arrays were then characterized by AFM. In the case of arrays composed of immunoglobulin G (IgG) patterns, the reaction of the array with rabbit antibody to mixtures of proteins was studied by AFM.

Lysozyme, an ellipsoidal shaped protein (4.5 nm by 3.0 nm by 3.0 nm), (*17*) cleanly assembled on the MHA nanopatterns, as evidenced by contact and tapping mode AFM (Fig. 1, B to D), respectively (*18*). Note that there is almost no evidence of nonspecific

[1]Northwestern University, Department of Chemistry and Center for Nanofabrication and Molecular Self-Assembly, 2145 Sheridan Road, Evanston, IL 60208, USA. [2]University of Chicago, Department of Chemistry and the Institute for Biophysical Dynamics, 5735 South Ellis, Chicago, IL 60637, USA.

*To whom correspondence should be addressed. E-mail: camirkin@chem.northwestern.edu; for cell adhesion work: mmrksich@midway.uchicago.edu

protein adsorption on the array and that height profiles suggest that between one and two layers of protein adsorb at each MHA site (*19*). The height distribution observed in the image is likely due to the different orientations the protein can adopt on the MHA-coated surface (Fig. 1C, inset). Finally, the protein can be assembled in almost any array configuration, including lines and grids (Fig. 1D).

IgG, which has substantially different dimensions (Y-shape, height = 14.5 nm, width = 8.5 nm, thickness = 4.0 nm) (*20, 21*), exhibited qualitatively similar adsorption characteristics (*19*) (Fig. 3). The height profile of an IgG nanoarray shows that each IgG feature is 6.5 ± 0.9 nm (n = 10) high, which is consistent with a single monolayer of the protein adsorbed onto the MHA features and is comparable to what others have seen for macroscopic features (*10–13*).

We addressed the issue of nonspecific binding by incubating a nanoarray of rabbit IgG in a four-component aqueous protein solution (10 mM Tris buffer, pH 7.3) containing lysozyme, Retronectin, goat/sheep antibody to IgG (anti-IgG), and human anti-IgG (each at 10 μg/ml) for 1 hour. A comparison of the AFM images of the array before and after treatment with this solution shows no evidence of protein binding to the array and almost no detectable nonspecific binding to the passivated, inactive areas of the substrate (compare Fig. 3, A and B). When a nanoarray of rabbit IgG was treated with a solution containing lysozyme, goat/sheep anti-IgG, human anti-IgG, and rabbit anti-IgG (concentration of each was 10 μg/ml) for 1 hour, each of the active features of the array increase in height from 6.5 ± 0.9 nm (n = 10) to 12.1 ± 1.3 nm (n = 10) (compare Fig. 3, C and D). This almost doubling in height is consistent with a 1:1 reaction between the two protein structures. These experiments show that regardless of the orientations of the IgG within the nanoscopic features, the proper orientation can be adopted under these conditions to react with the anti-IgG in a complex protein solution. Thus, the proteins maintained biological activity after adsorption.

These protein nanoarrays also can be used for studying other biological interactions, such as cell adhesion, on a much finer length scale than what is possible with conventional micro- and nanofabrication techniques. We fabricated an array of Retronectin, a cellular adhesion protein that is a recombinant fragment of fibronectin containing the central cell-binding domain, the heparin-binding domain II, and a CS1 site (Fig. 4). The adhesion of cells to Retronectin is mediated by the binding of integrin receptors to peptides found within the extracellular matrix protein (*22*). After adhesion and spreading of a cell, the integrin receptors cluster into aggregates that recruit the assembly of several cytoplasmic proteins at the membrane into a complex termed the focal adhesion. These focal adhesion sites serve to regulate adhesion-de-

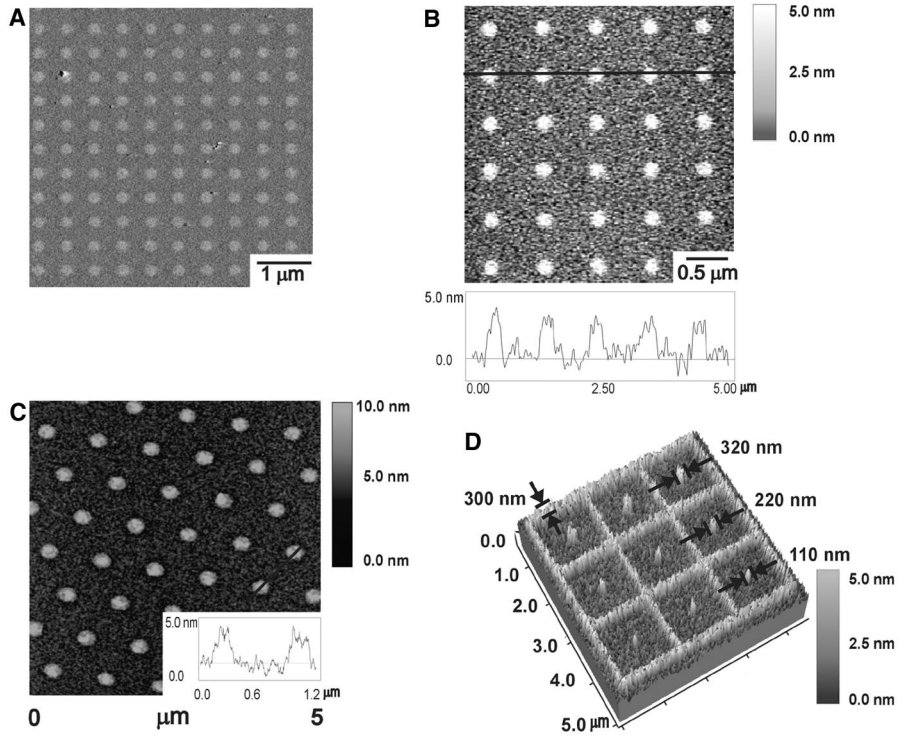

Fig. 1. AFM images and height profiles of lysozyme nanoarrays. (**A**) Lateral force image of an 8 μm by 8 μm square lattice of MHA dots deposited onto an Au substrate. The array was imaged with an uncoated tip at 42% relative humidity (scan rate = 4 Hz). (**B**) Topography image (contact mode) and height profile of the nanoarray after lysozyme adsorption. A tip-substrate contact force of 0.2 nN was used to avoid damaging the protein patterns with the tip. (**C**) A tapping mode image (silicon cantilever, spring contant = ~40 N/m) and height profile of a hexagonal lysozyme nanoarray. The image was taken at a scan rate of 0.5 Hz to obtain high resolution. (**D**) Three-dimensional topographic image of a lysozyme nanoarray, consisting of a line grid and dots with intentionally varied feature dimensions. Imaging was done in contact mode as described in (B).

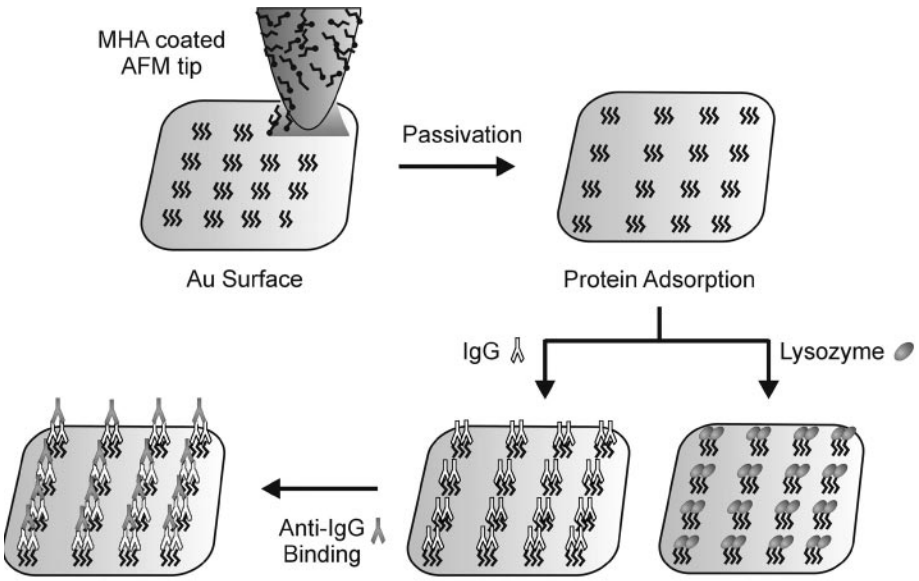

Fig. 2. Diagram of proof-of-concept experiments, in which proteins were absorbed on preformed MHA patterns. The resulting protein arrays were then characterized by AFM.

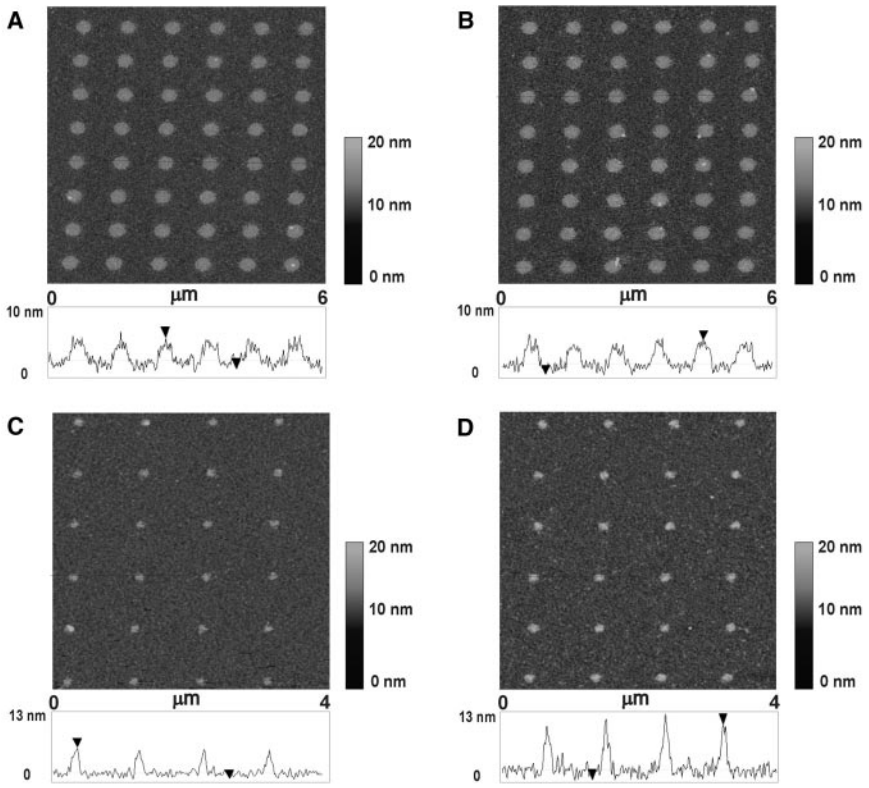

Fig. 3. AFM tapping mode image and height profile of rabbit IgG assembled onto an MHA dot array generated by DPN before (**A**) and after (**B**) exposure to a solution containing lysozyme, Retronectin, goat/sheep anti-IgG, and human anti-IgG. An IgG nanoarray before (**C**) and after (**D**) treatment with a solution containing lysozyme, goat/sheep anti-IgG, human anti-IgG, and rabbit anti-IgG. All images were taken at a 0.5-Hz scan rate in tapping mode.

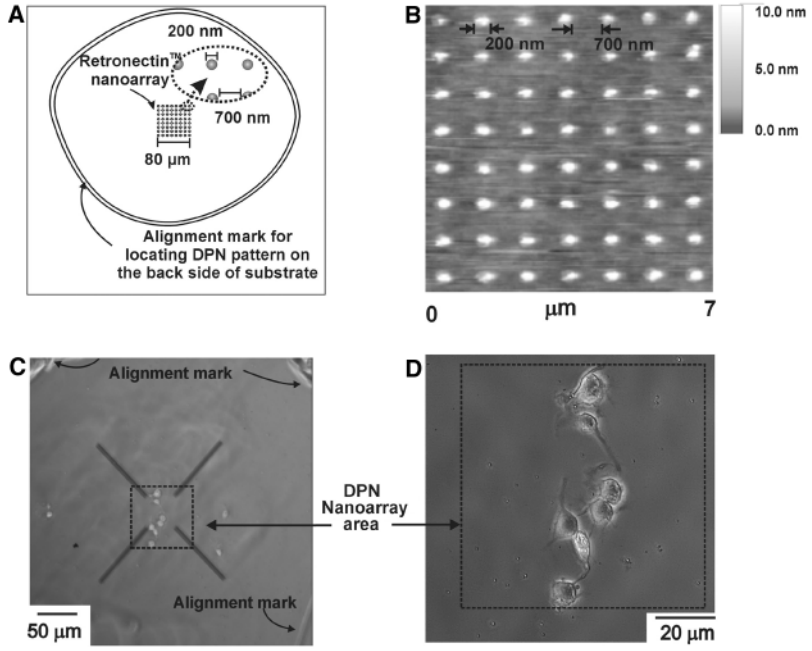

Fig. 4. (**A**) Diagram describing the cell adhesion experiment on the DPN-generated pattern. The total patterned area is 6400 μm^2. The alignment marks were generated by scratching a circle into the backside of the Au-coated glass substrate. (**B**) Topography image (contact mode) of the Retronectin protein array. Imaging conditions were the same as in Fig. 1B. (**C**) Large-scale optical microscope image showing the localization of cells in the nanopatterned area. (**D**) Higher resolution optical image of the nanopatterned area, showing intact cells.

pendent signaling processes and also play an important mechanical role by connecting the actin cytoskeleton structure to the substrate. An understanding of how adhesion and signaling of cells depend on the sizes and distributions of focal adhesions has been limited in patterning studies of immobilizing proteins to 1-μm patches, which do not have the resolution necessary for characterizing the sizes of focal adhesions that are necessary for normal cell adhesion (*4*). Whereas current studies reveal that focal adhesions have sizes on the micrometer length scale, the lack of higher resolution patterning methods has prevented direct examination of the range of sizes that constitute active focal adhesions (*23*).

To test whether cells can adhere to protein nanoarrays with features well below 1 μm, we used DPN to pattern MHA into a square array of dots that are 200 nm in diameter and separated by 700 nm (Fig. 4A) (*24*). Like the other proteins, AFM images (*19*) showed that the Retronectin adsorbed almost exclusively on the MHA pattern (Fig. 4B). The protein nanoarray was then immersed for 12 hours in a Dulbecco's Modified Eagle Medium (DMEM) solution with 10% bovine calf serum, which contained the 3T3 Swiss fibroblast cells (20,000 cells/ml). The arrays were then gently rinsed with phosphate buffered saline (PBS) and studied by optical microscopy. Significantly, cells only attach to the patterned region of the substrate and spread, but not completely, into a more flattened morphology. This morphology is a direct consequence of the sizes and spacings of the patterned protein, because cells placed on a nonpatterned substrate were well spread. Thus, submicrometer features can support cell adhesion and point toward the importance of a way of systematically identifying the relation between nanofeature size and composition in studies of cell adhesion and other related processes.

The ability to make protein nanoarrays on a surface with well-defined feature size, shape, and spacing should increase the capabilities of researchers studying the fundamental interactions between biological structures (cells, complementary proteins, and viruses) and surfaces patterned with proteins. Although we have explored only three proof-of-concept systems, we expect that it can be extended, with straightforward modifications of the aforementioned protocols, to a wide range of biomolecular structures and that the resolution of the technique, once optimized, should compare well with that of conventional DPN (10 nm) (*25–27*).

References and Notes

1. G. MacBeath, S. L. Schreiber, *Science* **289**, 1760 (2000).
2. A. S. Blawas, W. M. Reichert, *Biomaterials* **19**, 595 (1998).
3. R. S. Kane *et al.*, *Biomaterials* **20**, 2363 (1999).
4. C. S. Chen *et al.*, *Science* **276**, 1425 (1997).

5. S. P. A. Foder *et al.*, *Science* **251**, 767 (1991).
6. M. Schena *et al.*, *Proc. Natl. Acad. Sci. U.S.A.* **93**, 10614 (1996).
7. D. V. Nicolau, T. Tauguchi, H. Taniguchi, S. Yoshikawa, *Langmuir* **14**, 1927 (1998).
8. M. Mrksich *et al.*, *Proc. Natl. Acad. Sci. U.S.A.* **93**, 10775 (1996).
9. A. A. Bergman *et al.*, *Langmuir* **14**, 6785 (1998).
10. M. E. Browning-Kelley, K. Waud-Mesthrige, V. Hari, G.-Y. Liu, *Langmuir* **13**, 343 (1997).
11. K. Waud-Mesthrige, S. Xu, N. A. Amro, G.-Y. Liu, *Langmuir* **15**, 8580 (1999).
12. K. Waud-Mesthrige *et al.*, *Biophys. J.* **80**, 1891 (2001).
13. J. R. Kenseth, J. A. Harnisch, V. W. Jones, M. D. Porter, *Langmuir* **17**, 4105 (2001).
14. D. L. Wilson *et al.*, *Proc. Natl. Acad. Sci. U.S.A.* **98**, 13660 (2001).
15. K. L. Prime, G. M. Whitesides, *Science* **252**, 1164 (1991).
16. G. P. Lopez *et al.*, *J. Am. Chem. Soc.* **115**, 10774 (1993).
17. C. C. F. Blake *et al.*, *Nature* **206**, 757 (1965).
18. All DPN patterning and contact mode imaging experiments were done with a ThermoMicroscopes CP AFM interfaced with customized software and conventional Si_3N_4 cantilevers (Thermo Microscopes sharpened Microlever A, force constant = 0.05 N/m). Tapping mode images were taken with a Nanoscope IIIa and MultiMode microscope from Digital Instruments. Unless otherwise mentioned, all DPN patterning experiments were conducted at 40% relative humidity and 24°C with a tip-substrate contact force of 0.5 nN. A 90-μm scanner, with closed-loop scan control, was used for all DPN experiments to minimize piezo tube drift and alignment problems. Finally, attempts to use bovine serum albumin (BSA) as a passivation agent, instead of 11-mercaptoundecyl-tri(ethylene glycol), proved inferior and led to substrates with significant nonspecific binding of both proteins.
19. Supplementary material is available on *Science* Online at www.sciencemag.org/cgi/content/full/1067172/DC1.
20. E. W. Silverton, M. A. Navia, D. R. Davies, *Proc. Natl. Acad. Sci. U.S.A.* **74**, 5140 (1977).
21. The basic structure of monomeric IgG consists of two identical halves; each half comprises a heavy and a light chain. The heavy chains form the base of the "Y" and are COOH-terminated, and the light chains form the arms of the "Y" and are NH_2-terminated. Hence, the data is consistent with the arms of the "Y" interacting with the MHA nanofeatures and the anti-IgG complexing to the exposed base of the "Y."
22. F. Kimizuka *et al.*, *J. Biochem.* **110**, 284 (1991).
23. J. C. Adams, *Cell. Mol. Life Sci.* **58**, 371 (2001).
24. These arrays were passivated with 11-mercaptoundecyl-tri(ethylene glycol), and then modified with Retronectin by placing a 50-μl droplet of the protein (50 μg/ml) dissolved in PBS solution on the patterned surface for 30 min. The substrate was then repeatedly rinsed with PBS and NANOpure water.
25. R. D. Piner, J. Zhu, F. Xu, S. Hong, C. A. Mirkin, *Science* **283**, 661 (1999).
26. S. Hong, J. Zhu, C. A. Mirkin, *Science* **286**, 523 (1999).
27. S. Hong, C. A. Mirkin, *Science* **288**, 1808 (2000).

28. C.A.M. acknowledges the Air Force Office of Scientific Research, the Defense Advanced Research Projects Agency (DARPA), and the NSF for support of this research. J.C.S. and M.M. acknowledge DARPA and NIH for generous support.

16 October 2001; accepted 28 January 2002
Published online 7 February 2002;
10.1126/science.1067172
Include this information when citing this paper.

Niobium-Zirconium Chronometry and Early Solar System Development

Maria Schönbächler,[1]* Mark Rehkämper,[1] Alex N. Halliday,[1] Der-Chuen Lee,[1] Michèle Bourot-Denise,[3] Brigitte Zanda,[3,4] Bodo Hattendorf,[2] Detlef Günther[2]

Niobium-92 (^{92}Nb) decays to zirconium-92 (^{92}Zr) with a half-life of 36 million years and can be used to place constraints on the site of *p*-process nucleosynthesis and the timing of early solar system processes. Recent results have suggested that the initial ^{92}Nb/^{93}Nb of the solar system was high ($>10^{-3}$). We report Nb-Zr internal isochrons for the ordinary chondrite Estacado (H6) and a clast of the mesosiderite Vaca Muerta, both of which define an initial ^{92}Nb/^{93}Nb ratio of $\sim10^{-5}$. Therefore, the solar system appears to have started with a ratio of $<3 \times 10^{-5}$, which implies that Earth's initial differentiation need not have been as protracted as recently suggested.

Some extinct radionuclides were sufficiently abundant at the start of the solar system that they produced variations in the abundance of their daughter isotopes in early-formed objects (*1*). Such nuclides provide information about late-stage presolar nucleosynthetic sites and the time scales over which the early solar system formed and first differentiated (*2–4*). Of considerable interest in this regard is ^{92}Nb, which decays by electron capture with a half-life of 36 ± 3 million years (My) to ^{92}Zr (*5, 6*). ^{92}Nb is a shielded nuclide that forms by the *p*-process only. The *p*-process is a nucleosynthetic process that occurs in supernovae and produces proton-rich nuclides. Therefore, the initial abundance of ^{92}Nb provides information on stellar nucleosynthesis before the start of the solar system.

Both Nb and Zr are refractory and lithophile, except under reducing conditions when Nb may become siderophile (*7*). Within the Earth the dominant Nb/Zr fractionation mechanisms are silicate partial melting (*8*) and the crystallization of accessory minerals such as zircon, ilmenite, and rutile. The Zr isotopic compositions of early reservoirs can therefore vary in response to early differentiation processes and can help in dating planetary differentiation, if the initial abundance of ^{92}Nb (or ^{92}Nb/^{93}Nb) was sufficiently high.

Early results demonstrated that the initial ^{92}Nb/^{93}Nb of the solar system was <0.007 (*9*). Evidence of formerly live ^{92}Nb was first identified in a Nb-rich rutile from the iron meteorite Toluca (*10*). An initial ^{92}Nb/^{93}Nb of 1.6 ($\pm$0.3) $\times$ 10^{-5} was inferred. More recently, three studies using a multiple-collector inductively coupled plasma mass spectrometer (MC-ICPMS) proposed that the initial ^{92}Nb/^{93}Nb ratio of the solar system was higher by two orders of magnitude ($\sim10^{-3}$) (*11–13*). Such a high value limits the possible sites for *p*-process nucleosynthesis and places specific constraints on the time scales for the development of differentiated reservoirs on the Earth and Moon. For example, it has been argued that large silicate reservoirs in the Earth and Moon formed >50 My after the start of the solar system (*12*). However, such a result requires that the Toluca rutile grew very late (>200 My). In contrast, a combined Zr isotopic and U-Pb age study of an early zircon from a eucrite implied that the initial ^{92}Nb/^{93}Nb ratio was $<10^{-4}$ (*14*).

Here, we used the internal isochron approach to determine the initial ^{92}Nb/^{93}Nb ratio of the solar system. Two meteorites were studied in which ilmenite with high Nb/Zr is in textural equilibrium with other phases having intermediate Nb/Zr. Because the half-life of ^{92}Nb is long (36 My) and the level of uncertainty concerning the initial solar system abundance is more than two orders of magnitude, the critical concern is not the exact age of the meteorite (provided it is reasonably early) but the acquisition of a reliable isochron from a cogenetic suite of phases that remained undisturbed after their formation. Therefore, we used the equilibrated but only weakly shocked (S1) H6 ordinary chondrite Estacado, which has a single generation of ilmenite, and a eucritic clast from the mesosiderite Vaca Muerta.

Using a Nu Plasma MC-ICPMS, we were able to measure ε^{92}Zr with an external precision of ±0.3 ε units (2σ standard deviation) for samples with only 50 ng of Zr (*15*). The Nb/Zr ratios were determined by inductively coupled plasma dynamic reaction cell mass

[1]Institute of Isotope Geology and Mineral Resources, [2]Laboratory of Inorganic Chemistry, ETH Zürich, 8092 Zürich, Switzerland. [3]Museum national d'Histoire naturelle, 75005, Paris, France. [4]Rutgers University, Department of Geological Sciences, Wright Lab, Piscataway, NJ 08854-8066, USA.

*To whom correspondence should be addressed. E-mail: maria@erdw.ethz.ch